From Coherent to Fermionized Microwave Photons in a Superconducting Transmission Line

Alberto Tabarelli de Fatis,[1,*] Stephanie Matern,[1] Gianluca Rastelli,[1,2] and Iacopo Carusotto[1,2]
[1]Pitaevskii BEC Center, INO-CNR and Dipartimento di Fisica, Università di Trento, Via Sommarive 14, I-38123 Trento, Italy
[2]INFN-TIFPA, Trento Institute for Fundamental Physics and Applications, Via Sommarive 14, I-38123 Trento, Italy

(Received 19 January 2026; revised 12 May 2026; accepted 9 October 2026; published 3 November 2026)

We investigate superconducting transmission lines as a novel platform for realizing a quantum fluid of microwave photons in a propagating geometry. We anticipate that the strong photon-photon interactions provided by the intrinsic nonlinearity of Josephson junctions are sufficient to enter a regime of strongly interacting photons for realistic parameters. To prove the potential of this platform, we show that a suitable tapering of the transmission line parameters allows for the adiabatic conversion of an incident coherent field into a cold Tonks-Girardeau gas of fermionized photons close to its ground state. Signatures of the strong correlations are visible in the correlation properties of the transmitted light.

DOI: 10.1103/g262-dlhf

Leveraging the effective photon-photon interactions stemming from the optical nonlinearity of the medium, quantum fluids of light have emerged as a promising new system to study many-body physics in novel regimes [1,2]. While most experiments so far are in a weak interaction regime, first steps toward strongly correlated regimes have been made with the observation of a Mott insulator state [3], a spectroscopical study of a system of impenetrable photons [4], and the realization of few-body fractional quantum Hall liquids [5,6]. These experiments have mostly been carried out in cavity configurations where losses are intrinsically needed to establish the steady state and to measure the quantum state of the photon gas.

On the other hand, systems with propagating geometries [7] can be ideally operated in regimes with no losses where propagation is described by unitary evolution under the exchange of the role of spatial and temporal coordinates [8,9]. Most experiments so far have used visible light and focused on weakly interacting gases, with observations of superfluidity [10], thermalization, and condensation phenomena [11,12]. At the same time, pioneering works have started exploring regimes with stronger nonlinearities, leading to the observation of marked antibunching and few-photon bound states [13,14]. However, the observation of strongly quantum correlated many-body states has so far remained elusive.

Capitalizing on the development of circuit-QED technologies [15], superconducting nonlinear transmission lines have experienced dramatic advances in recent years, e.g., in view of realizing quantum limited amplifiers—the so called traveling wave parametric amplifiers (TWPA) [16]—and generating squeezed states of microwave fields [17]. The design flexibility of state-of-the-art TWPAs and the strong nonlinearities provided by Josephson junction (JJ) elements [18] make these devices a natural platform to study and generate strongly correlated gases of microwave photons.

In this Letter we derive an effective quantum theory for the propagation of the microwave photon field in a superconducting transmission line in terms of a unitary Hamiltonian evolution, which provides a powerful tool for predicting quantum optical features. As a proof of concept to demonstrate the potential of our approach, we show how a suitable tapering of the transmission line parameters allows for converting a monochromatic and fully coherent incident radiation into a one-dimensional Tonks-Girardeau (TG) gas of impenetrable photons [19,20].

While the incident coherent field is straightforwardly obtained with commercially available microwave generators, the TG gas is a remarkable many-body state where strong optical nonlinearities make bosonic photons behave analogously to fermionic particles. In contrast to the strong size limitations of TG gases of ultracold atomic clouds [21,22], our scheme can generate a TG gas of an indefinitely large number of photons just by operating the device for a macroscopically long time and, at the same time, offers direct access to the correlation functions of the TG gas. Beyond antibunching, distinct signatures of the fermionized behavior [23] of strongly interacting photons appear as Friedel oscillations in the second-order correlation function. The correlated nature of the gas is also visible in the speed of the light-cone propagation of excitations

*Contact author: a.tabarellidefatis-2@unitn.it

Published by the American Physical Society under the terms of the Creative Commons Attribution 4.0 International license. Further distribution of this work must maintain attribution to the author(s) and the published article's title, journal citation, and DOI.

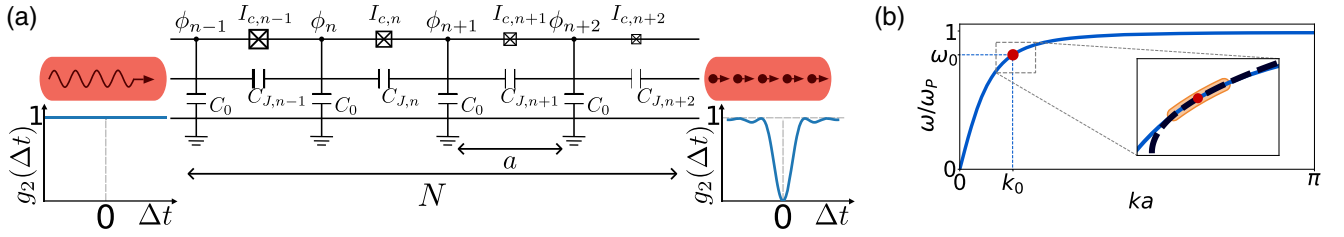


FIG. 1. (a) Sketch of the transmission line model, composed of unit cells of length a with a capacitor C_0 to ground and a series of N JJs characterized by a critical current $I_{c,n}$ and a capacitance $C_{J,n}$, whose values are tapered along the propagation. The monochromatic coherent incident radiation, characterized by a flat second order photon correlation function $g_2(\Delta t)$, is converted into a gas of fermionized photons, with a $g_2(\Delta t)$ showing antibunching and Friedel oscillations. (b) Sketch of the linear dispersion relation of the transmission line (solid blue line), together with the quadratic approximation around the carrier frequency ω_0 (dashed black line). The incident monochromatic field is localized in frequency (red dot), whereas the fermionized photon gas after propagation has a finite spread in frequency (orange area).

after a sudden ramp [24], which follows the prediction of the Lieb-Liniger (LL) model [25,26]. Realization of the TG gas represents a first step toward the realization of many other strongly correlated states of light, such as a macroscopically sized Mott insulator of photons. Beyond fundamental science, the resulting array of single-photon wave packets opens remarkable opportunities for quantum technologies.

We model a nonlinear superconducting transmission line based on JJs, as sketched in Fig. 1(a), with the Lagrangian [27]

$$L_{\text{circuit}} = \frac{1}{2}\sum_n C_{0,n}\dot{\phi}_n^2 + \frac{1}{2}\sum_n C_{J,n}(\dot{\phi}_{n+1}-\dot{\phi}_n)^2 + \frac{\Phi_0}{2\pi}\sum_n I_{c,n}\cos\left[\frac{2\pi}{\Phi_0}(\phi_{n+1}-\phi_n)\right]. \quad (1)$$

The flux variables ϕ_n are defined such that the superconducting phase difference across a JJ at position n is $\varphi_n = 2\pi(\phi_{n+1}-\phi_n)/\Phi_0$, with $\Phi_0 = h/2e$ being the magnetic flux quantum. Furthermore, $I_{c,n}$ is the critical current of the JJ, $C_{J,n}$ is its capacitance, and $C_{0,n}$ is the capacitance to ground. Assuming a spatially homogeneous line and restricting to quadratic terms in the fields in the Lagrangian, we obtain the linear dispersion relation of the transmission line, plotted in Fig. 1(b),

$$\omega^2 = \omega_P^2 \frac{4c\sin^2(\frac{ka}{2})}{1+4c\sin^2(\frac{ka}{2})}. \quad (2)$$

Here, we assumed the unit cells to have constant length a, $c = C_J/C_0$, $\omega_P = 1/\sqrt{L_J C_J}$ is the plasma frequency, and $L_J = \Phi_0/(2\pi I_c)$ is the inductance of the JJ.

Nonlinear effects can be modeled assuming a low field amplitude. This amounts to expanding the cosine in the Lagrangian of Eq. (1) up to the fourth order in the small parameter ϕ_n/Φ_0 and leads to the action $S = S_L + S_{NL}$, which consists of a linear and nonlinear part, with

$$S_L = \int dt\left[\frac{C_0}{2}\sum_n \dot{\phi}_n^2 + \frac{C_J}{2}\sum_n(\dot{\phi}_{n+1}-\dot{\phi}_n)^2 - \frac{1}{2L_J}\sum_n(\phi_{n+1}-\phi_n)^2\right],$$
$$S_{NL} = \int dt\left[\frac{1}{24L_J}\left(\frac{2\pi}{\Phi_0}\right)^2\sum_n(\phi_{n+1}-\phi_n)^4\right]. \quad (3)$$

Note that this form holds for generic transmission lines involving components whose current-phase relation is $I(\phi+\phi^*) = \phi/L_J - \gamma\phi^3$, such as superconducting quantum interference devices (SQUIDs) [28], Superconducting Nonlinear Asymmetric Inductive eLements (SNAILs) [29] operated in suitable regimes where three-wave mixing is negligible, or other possible architectures [30].

By introducing a continuous spatial coordinate $z = an$ along the propagation direction and expanding the field ϕ_n in Fourier components $\phi(z,t) = \int dk/(2\pi)\int d\omega/(2\pi)A(k,\omega)e^{i(kz-\omega t)}$, with $A(-k,-\omega) = A^*(k,\omega)$, we obtain for the linear action

$$S_L = -\frac{C_0}{2a}\int\frac{dk}{2\pi}\int\frac{d\omega}{2\pi}|A(k,\omega)|^2 F(k,\omega). \quad (4)$$

Here,

$$F(k,\omega) = -\omega^2\left[1+4c\sin^2\left(\frac{ka}{2}\right)\right] + 4c\omega_P^2\sin^2\left(\frac{ka}{2}\right) \quad (5)$$

describes the linear dispersion relation via $F(k,\omega) = 0$. In the following, we restrict to circuit parameters inside the superconducting phase of the Josephson transmission line, in order to avoid the insulating behavior [31]. This roughly corresponds to working in regimes where the charging energy of the ground capacitance is comparable or smaller than the Josephson energy (see End Matter).

Within the slowly varying envelope approximation (SVEA), we can expand $F(k,\omega)$ around the carrier wave vector k_0 and frequency ω_0 [see Fig. 1(b)]:

$$S_L \approx -\frac{C_0}{a}\left(\frac{\partial F}{\partial k}\right)_{(k_0,\omega_0)} \int \frac{d(\delta k)}{2\pi}\frac{d(\delta\omega)}{2\pi}|\tilde{A}(\delta k,\delta\omega)|^2 \times \left(\delta k - \frac{1}{v_g}\delta\omega - \frac{D}{2}\delta\omega^2\right), \tag{6}$$

with $\tilde{A}(\delta k = k - k_0, \delta\omega = \omega - \omega_0) = A(k,\omega)$. The group velocity and curvature are evaluated at (k_0,ω_0) as $v_g = \partial_k\omega$ and $D = \partial_\omega^2 k = -v_g^{-3}\partial_k^2\omega$, and can be expressed in terms of derivatives of F via explicit formulas (see Supplemental Material [32]).

Introducing the slowly varying field ϕ_0 defined via $\phi(z,t) = e^{i(k_0 z-\omega_0 t)}\phi_0(z,t) + \text{c.c.}$ and computing the nonlinear term within the zeroth order SVEA, the total action reads as

$$S = \int d\tau \int d\zeta\, \mathcal{C}\left[i\hbar\phi_0^*\partial_\tau\phi_0 + i\hbar\frac{\bar{v}_g^2}{v_g}\phi_0^*\partial_\zeta\phi_0 + \frac{\hbar\bar{v}_g^3 D}{2}|\partial_\zeta\phi_0|^2 - \frac{\tilde{g}}{2}|\phi_0|^4\right]. \tag{7}$$

Here, we exchanged the role of space and time via the change of variables $\zeta = t\bar{v}_g$ and $\tau = z/\bar{v}_g$, with $\bar{v}_g$ being an (arbitrarily chosen [36]) reference velocity and $\mathcal{C}$ being an overall normalization factor [see Eq. (A1)], which plays a crucial role in the quantum theory since it modifies the commutation relations.

We note that Eq. (7) is the action of a nonlinear Schrödinger equation [37] with a drift velocity term, which can be removed by a change of variables $\zeta' = \zeta - \bar{v}_g^2\int_0^\tau v_g^{-1}(\tau')d\tau'$. In the following we consider that the circuit parameters slowly vary with the position z along the transmission line, so all parameters in our action slowly depend on the effective time τ.

From the action in Eq. (7) we derive an effective quantum theory by imposing equal-τ commutation relations on the field $\hat{\phi}_0$ and its conjugate momentum [8,9]:

$$[\hat{\phi}_0(\zeta,\tau), \hat{\Pi}_{\phi_0}(\zeta',\tau)] = i\hbar\delta(\zeta-\zeta'). \tag{8}$$

Introducing the field operator,

$$\hat{\Psi}(\zeta,\tau) = \sqrt{\mathcal{C}(\tau)}\hat{\phi}_0(\zeta,\tau), \tag{9}$$

satisfying bosonic commutation relations $[\hat{\Psi}(\zeta,\tau), \hat{\Psi}^\dagger(\zeta',\tau)] = \delta(\zeta-\zeta')$, one obtains a Hamiltonian in the usual form of a one-dimensional Bose gas [23] with contact interactions of strength $g(\tau) = \tilde{g}/\mathcal{C}(\tau)$ and mass $m = -\hbar/(\bar{v}_g^3 D)$ [39]:

$$\hat{H} = \int_{-\infty}^{\infty} d\zeta\left[-\frac{\hbar^2}{2m}\hat{\Psi}^\dagger(\zeta)\frac{\partial^2}{\partial\zeta^2}\hat{\Psi}(\zeta) + \frac{g}{2}\hat{\Psi}^{\dagger 2}(\zeta)\hat{\Psi}^2(\zeta)\right]. \tag{10}$$

For repulsive interactions the eigenstates of this LL Hamiltonian [25,26] are determined by the dimensionless interaction parameter $\gamma = mg/(\hbar^2\rho)$, where ρ is proportional to the incident photon flux, as discussed later. As a peculiarity of our one-dimensional geometry, the impact of interactions increases for decreasing density ρ. In the strong interaction limit $\gamma \gg 1$ [40], the Bose gas approaches the $\gamma \to \infty$TG regime, where it displays an effective fermionic behavior [20].

Moving back to our specific superconducting transmission line model, we first note that, according to the explicit formulas given in the End Matter, both the mass m and the interaction strength g are negative: modulo an overall sign in the Hamiltonian (which has no effect on the dynamics of an isolated system), the physics then recovers the one of a repulsively interacting gas. Second, the density ρ of the Bose gas can be related to the incident photon flux by $\rho = \Phi_{\text{ph}}/\bar{v}_g$ (see End Matter): the t-translationally invariant stationary states under our monochromatic pump correspond to a spatially homogeneous gas in ζ with no limitation on its size. Furthermore, the two-time correlation functions $g_{1,2}(\Delta t = t_2 - t_1, z = L)$ after propagation along a transmission line of length $L = Na$ are given by the corresponding two-position correlation functions $g_{1,2}[\Delta\zeta = \zeta_2 - \zeta_1 = \bar{v}_g(t_2 - t_1), \tau = L/\bar{v}_g]$ of the Bose gas. Finally, while $g_{1,2}$ is ideally measured with single-photon detectors, schemes to also measure it for microwave photons using linear amplifiers and quadrature amplitude detectors have been developed [41–43].

According to the general theory of the TG gas [23], photon fermionization is apparent in the second-order photon correlations of the ground state

$$g_2^{TG}(\Delta t) = 1 - \left(\frac{\sin(\pi\Phi_{\text{ph}}\Delta t)}{\pi\Phi_{\text{ph}}\Delta t}\right)^2: \tag{11}$$

a full antibunching is visible at short delays Δt, followed by Friedel oscillations at larger Δt. While the antibunching can be explained in terms of a two-photon blockade mechanism [13,42] persisting at finite temperatures, the Friedel oscillations are a true many-body effect resulting from the quantum correlated nature of the ground state. Their many-body origin is apparent in the value of their frequency, which is set by the photon flux Φ_{ph} and corresponds to the Fermi wave vector. This is in contrast to resonance fluorescence [44], where the oscillations in g_2 are set by the Rabi frequency proportional to the amplitude of the incident electric field. On the other hand, the first order correlation function in the ground state monotonically decays at large time delays as a power law [23]:

$$g_1^{TG}(\Delta t) \sim \frac{1}{\sqrt{\pi\Phi_{\text{ph}}|\Delta t|}}. \tag{12}$$

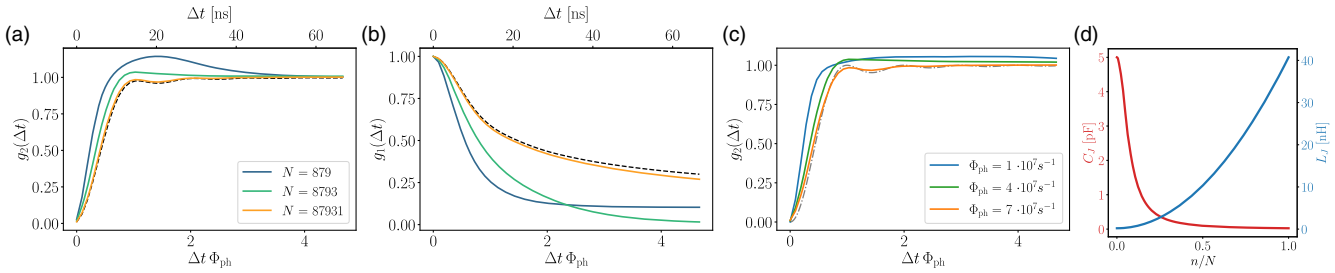


FIG. 2. Second (a),(c) and first (b) order correlation function of the microwave field transmitted by the transmission line sketched in Fig. 1(a). The ramp of the circuit parameters is shown in (d), with a constant plasma frequency of $\omega_p = 1/\sqrt{L_J C_J} = 2\pi \times 5$ GHz, a constant ground capacitance $C_0 = 30$ fF, and an incident coherent field frequency $\omega_0/2\pi = 4.25$ GHz. The incident photon rate is $\Phi_{\rm ph} = 7 \times 10^7$ s^{-1} in (a) and (b) and varies according to the legend in (c). The number of cells N of the transmission line varies according to the legend in (a) and (b) and is $N = 87931$ for (c). The dashed black line in (a) and (b) is the numerical ground state prediction computed numerically at the final value $\gamma \approx 33.2$, whereas the dashed-dotted line in (c) is the analytical TG result in the $\gamma = \infty$ limit.

In order to observe such a quantum correlated many-body state, we propose slowly varying the nonlinear properties of the transmission line to adiabatically convert an incident monochromatic and fully coherent radiation of frequency ω_0 into a TG gas of fermionized microwave photons close to the many-body ground state. In stark contrast to most experiments so far [7,12,13], which involve fast variations of the optical nonlinearity upon entering the medium and thus lead to highly excited states, we propose slowly varying the parameters of the transmission line in space to adiabatically increase the LL parameter γ.

As the LL model is gapless [26] and the adiabatic theorem cannot be directly applied [45], we employ τ-dependent infinite tensor-network algorithms [32–34] to numerically simulate the full many-body problem of the microwave propagation along the transmission line. The specific adiabatic ramp in the temporal variable τ used in the numerics corresponds to the spatial variation of the circuit parameters along the transmission line sketched in Fig. 1(a): C_0 and $\omega_P = 1/\sqrt{L_J C_J}$ are kept constant while L_J and C_J are changed as shown in Fig. 2(d).

Note that our theory assumes from the outset that light is unidirectionally propagating along the transmission line and no reflections occur at its terminations. This can be ensured by impedance matching the transmission line with the input-output lines, e.g., with a suitable further tapering. Note that this latter tapering at the edges of the line can be done on a length scale of the order of the microwave wavelength, which imposes a much less severe constraint on the transmission line length than the many-body adiabaticity discussed above.

In Fig. 2, we show the correlation properties of the stationary microwave field that emerges after propagation along the tapered transmission line. In the figures, the propagation length is measured in terms of the number of cells N in the transmission line, which does not depend on the physical size a of the cell. The second order correlation function g_2 is shown in Fig. 2(a) for increasing values of the transmission line length but a fixed shape of the ramp profile. The short distance antibunching due to the repulsive contact interactions is visible in all curves, while the Friedel oscillations typical of the TG ground state [Eq. (11)] are well visible for the longest transmission line. This indicates that the gapless spectrum does not prevent the adiabatic evolution from approaching the ground state provided the transmission line is sufficiently long. The good agreement with the exact ground state at the final γ value is a quantitative verification of the efficiency of our adiabatic preparation scheme. Going deeper into the $\gamma \to \infty$TG limit would only slightly increase the amplitude of Friedel oscillations (see End Matter). The accurate preparation of the TG ground state is further illustrated in the plot of the first order correlation function shown in Fig. 2(b): for the longest transmission line, $g_1(\Delta t)$ approaches the power-law scaling of the TG ground state, again in good agreement with the exact ground state. Our specific simulations show that a number of cells around $N \approx 8.8 \times 10^4$ is sufficient to generate a TG gas close to the ground state. While this value is somehow larger than existing waveguide devices [46], much longer devices in the range of interest are routinely used for metrological applications [47].

In addition to fabricating longer transmission lines, the efficiency of the adiabatic ramp can also be improved by increasing the incident photon flux, as shown in Fig. 2(c), which softens the adiabaticity constraint on the length of the transmission line. This trick however faces limitations: the LL parameter γ decreases with $\Phi_{\rm ph}$ but has to remain in the $\gamma \gg 1$ strong interaction regime. On top of this, increasing $\Phi_{\rm ph}$ also increases the spread in the frequency distribution of the TG ground state, so the SVEA might eventually break down. A detailed discussion of the validity of our approximations for realistic parameters is given in the End Matter.

A further way to reduce the required length of the transmission line utilizes an overall scaling invariance of

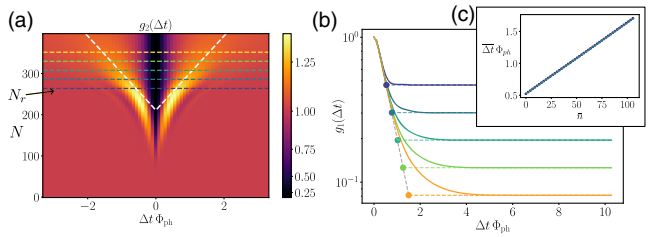


FIG. 3. Propagation of correlations after a moderately fast ramp during $N_r = 263$ cells [same ramp parameters as in Fig. 2(a)] followed by a uniform region with constant transmission line parameters. (a) Color plot of the second order photon correlation function $g_2(\Delta t)$ as a function of the propagation length in units of unit cells N. The color of the dashed lines corresponds to the different curves in (b); the arrow indicates the end of the ramp. The dashed white line indicates motion at the expected LL speed $2c_{LL}$. (b) Plots of the first order correlation function $g_1(\Delta t)$ at different propagation lengths n. The gray dashed line is an exponential fit of the short time decay of the longest-$\bar{z}$ curve; the horizontal dashed lines are the large Δt asymptotes. For each propagation length $\bar{n}$, the intersection between these two lines (colored points) defines $\overline{\Delta t}(\bar{n})$. The excellent agreement of the numerically extracted $\overline{\Delta t}(\bar{n})$ (dots) with the theoretically expected light-cone spreading at the LL speed c_{LL} (solid line) is shown in (c).

the Hamiltonian. The temporal variable τ can be reduced by a factor α by realizing a rescaled Hamiltonian αH, which can be achieved by uniformly increasing $L_J(\tau)$ by α while keeping C_0, $C_j(\tau)$, and r constant. Further improvements may be obtained by designing more complex transmission lines based on SQUIDs or SNAILs or opening a gap in the linear dispersion via a periodic modulation of the transmission line parameters.

As an alternative strategy, it is interesting to note that signatures of the quantum correlated nature of the strongly interacting photon gas are already visible for moderately short transmission lines. In Fig. 3 we show the correlation properties of the transmitted microwaves for a transmission line configuration displaying a relatively fast spatial ramp over N_r cells followed by a uniform region of varying length $\bar{n} = N - N_r$ (parameters in the caption). On top of the always visible antibunching at small Δt, an additional positive bump develops in $g_2(\Delta t)$ after the ramp, whose position shifts to larger Δt for growing $\bar{n}$, as shown in Fig. 3(a).

A related interesting dynamics is visible in the dynamics of the first order correlation function $g_1(\Delta t)$ during propagation shown in Fig. 3(b). Analogous to the recent atomic experiment of Ref. [48], immediately after the fast ramp the $g_1(\Delta t)$ correlation function retains memory of the initial coherent state, but its late-time value at large Δt progressively drops during propagation along the uniform part of the transmission line. As done in Ref. [48], we model $g_1(\Delta t)$ at small Δt with an exponential decay $g_1(\Delta t) \sim e^{-\Gamma \Delta t}$ and a Δt-independent (but n-dependent) value at large Δt. For each value of n, the transition point between the exponential and constant region is computed by locating in Fig. 3(b) the intersection point between the horizontal lines at the asymptotic constant values and the short-distance exponential decay.

As $\bar{n}$ increases, this transition point $\overline{\Delta t}$ between the two regions is expected to move outward according to the typical light cone spreading [49] $\bar{v}_g^2 \partial_{\bar{z}} \overline{\Delta t} = 2c_{LL}$ with $\bar{z} = a\bar{n}$. In contrast to the weakly interacting fluids of recent atomic [48] or photonic [24] experiments, however, the light-cone expansion speed c_{LL} is here determined by the many-body LL model [25,26]. As shown in the inset of Fig. 3(c), the value of the speed extracted from the numerical data differs from the expected theoretical LL value by only 0.5%.

To summarize, we have developed a theory for the propagation of microwave photons in a strongly nonlinear superconducting transmission line. Exchanging the role of space and time, propagation along the line can be described in terms of the Hamiltonian evolution in the form of an interacting one-dimensional Bose gas. Using this theory we propose a scheme to generate a Tonks-Girardeau gas of impenetrable photons with effective fermionic properties. Using a suitable tapering of the transmission line, an adiabatic preparation of the ground state is anticipated; for faster ramps, signatures of strong quantum correlations are visible in the light-cone propagation of excitations at a speed determined by the Lieb-Liniger model of one-dimensional interacting bosons. As a key advantage with respect to cavity configurations, the continuous-wave operation of our propagating scheme allows for overcoming the limitations in the spatial size of the system and, thus, opens the way to realizing gases of a macroscopic number of photons.

As natural next steps, we plan to address more complex transmission line geometries with an optimized dispersion relation and more sophisticated SQUID or SNAIL elements. This will allow for reinforcing the adiabaticity condition and, in this way, reducing the requirement on the transmission line length. Even though our discussion was focused on a specific circuit-QED setup, our predictions are straightforwardly extended to generic strongly nonlinear waveguide systems, both in the microwave and optical regimes, including kinetic inductance devices [50], polaritons in solid-state systems [51–53], and Rydberg-EIT configurations in atomic gases [13,14]. As future perspectives, our approach can be used to explore degenerate gases of multiphoton bound states under attractive interactions [54] and strongly interacting Bose gases in multiwaveguide geometries in the presence of synthetic magnetic fields [55] to realize, for instance, two-dimensional fractional quantum Hall liquids of light.

Acknowledgments—We acknowledge useful discussions with Felix Ahrens, Giulio Cappelli, Nicolò Crescini,

Quentin Glorieux, Christian Johansen, Pierre-Élie Larré, Federica Mantegazzini, and Pasquale Scarlino. This work was supported by the Provincia Autonoma di Trento; the Q@TN Initiative; the National Quantum Science and Technology Institute through the PNRR MUR Project under Grant No. PE0000023-NQSTI, cofunded by the European Union—NextGeneration EU; and the Deutsche Forschungsgemeinschaft (DFG, German Research Foundation) via the Research Unit FOR 5688 under Project No. 521530974.

Data availability—There are no publicly available research data or software supporting this manuscript. Requests for further information or data should be sent to the authors.

[1] I. Carusotto and C. Ciuti, Quantum fluids of light, Rev. Mod. Phys. **85**, 299 (2013).
[2] I. Carusotto, A. A. Houck, A. J. Kollár, P. Roushan, D. I. Schuster, and J. Simon, Photonic materials in circuit quantum electrodynamics, Nat. Phys. **16**, 268 (2020).
[3] R. Ma, B. Saxberg, C. Owens, N. Leung, Y. Lu, J. Simon, and D. I. Schuster, A dissipatively stabilized Mott insulator of photons, Nature (London) **566**, 51 (2019).
[4] G. P. Fedorov, S. V. Remizov, D. S. Shapiro, W. V. Pogosov, E. Egorova, I. Tsitsilin, M. Andronik, A. A. Dobronosova, I. A. Rodionov, O. V. Astafiev, and A. V. Ustinov, Photon transport in a Bose-Hubbard chain of superconducting artificial atoms, Phys. Rev. Lett. **126**, 180503 (2021).
[5] L. W. Clark, N. Schine, C. Baum, N. Jia, and J. Simon, Observation of Laughlin states made of light, Nature (London) **582**, 41 (2020).
[6] C. Wang, F.-M. Liu, M.-C. Chen, H. Chen, X.-H. Zhao, C. Ying, Z.-X. Shang, J.-W. Wang, Y.-H. Huo, C.-Z. Peng *et al.*, Realization of fractional quantum Hall state with interacting photons, Science **384**, 579 (2024).
[7] Q. Glorieux, C. Piekarski, Q. Schibler, T. Aladjidi, and M. Baker-Rasooli, *Chapter four—paraxial fluids of light* (Academic Press, 2025), pp. 157–241, 10.1016/bs.aamop.2025.04.002.
[8] Y. Lai and H. A. Haus, Quantum theory of solitons in optical fibers. I. Time-dependent Hartree approximation, Phys. Rev. A **40**, 844 (1989).
[9] P.-E. Larré' and I. Carusotto, Propagation of a quantum fluid of light in a cavityless nonlinear optical medium: General theory and response to quantum quenches, Phys. Rev. A **92**, 043802 (2015).
[10] C. Michel, O. Boughdad, M. Albert, P.-É. Larré, and M. Bellec, Superfluid motion and drag-force cancellation in a fluid of light, Nat. Commun. **9**, 2108 (2018).
[11] M. Abuzarli, N. Cherroret, T. Bienaimé, and Q. Glorieux, Nonequilibrium prethermal states in a two-dimensional photon fluid, Phys. Rev. Lett. **129**, 100602 (2022).
[12] Q. Fontaine, T. Bienaimé, S. Pigeon, E. Giacobino, A. Bramati, and Q. Glorieux, Observation of the Bogoliubov dispersion in a fluid of light, Phys. Rev. Lett. **121**, 183604 (2018).
[13] T. Peyronel, O. Firstenberg, Q.-Y. Liang, S. Hofferberth, A. V. Gorshkov, T. Pohl, M. D. Lukin, and V. Vuletić, Quantum nonlinear optics with single photons enabled by strongly interacting atoms, Nature (London) **488**, 57 (2012).
[14] Q.-Y. Liang, A. V. Venkatramani, S. H. Cantu, T. L. Nicholson, M. J. Gullans, A. V. Gorshkov, J. D. Thompson, C. Chin, M. D. Lukin, and V. Vuletić, Observation of three-photon bound states in a quantum nonlinear medium, Science **359**, 783 (2018).
[15] A. Blais, A. L. Grimsmo, S. M. Girvin, and A. Wallraff, Circuit quantum electrodynamics, Rev. Mod. Phys. **93**, 025005 (2021).
[16] M. Esposito, A. Ranadive, L. Planat, and N. Roch, Perspective on traveling wave microwave parametric amplifiers, Appl. Phys. Lett. **119**, 120501 (2021).
[17] L. Zhong, E. P. Menzel, R. Di Candia, P. Eder, M. Ihmig, A. Baust, M. Haeberlein, E. Hoffmann, K. Inomata, T. Yamamoto, Y. Nakamura, E. Solano, F. Deppe, A. Marx, and R. Gross, Squeezing with a flux-driven Josephson parametric amplifier, New J. Phys. **15**, 125013 (2013).
[18] B. Josephson, Possible new effects in superconductive tunnelling, Phys. Lett. **1**, 251 (1962).
[19] L. Tonks, The complete equation of state of one, two and three-dimensional gases of hard elastic spheres, Phys. Rev. **50**, 955 (1936).
[20] M. Girardeau, Relationship between systems of impenetrable bosons and fermions in one dimension, J. Math. Phys. (N. Y.) **1**, 516 (1960).
[21] T. Kinoshita, T. Wenger, and D. S. Weiss, Observation of a one-dimensional Tonks-Girardeau gas, Science **305**, 1125 (2004).
[22] B. Paredes, A. Widera, V. Murg, O. Mandel, S. Fölling, I. Cirac, G. V. Shlyapnikov, T. W. Hänsch, and I. Bloch, Tonks–Girardeau gas of ultracold atoms in an optical lattice, Nature (London) **429**, 277 (2004).
[23] Y. Castin, Simple theoretical tools for low dimension Bose gases, J. Phys. IV France **116**, 89 (2004).
[24] J. Steinhauer, M. Abuzarli, T. Aladjidi, T. Bienaimé, C. Piekarski, W. Liu, E. Giacobino, A. Bramati, and Q. Glorieux, Analogue cosmological particle creation in an ultracold quantum fluid of light, Nat. Commun. **13**, 1 (2022).
[25] E. H. Lieb and W. Liniger, Exact analysis of an interacting Bose gas. I. The general solution and the ground state, Phys. Rev. **130**, 1605 (1963).
[26] E. H. Lieb, Exact analysis of an interacting Bose gas. II. The excitation spectrum, Phys. Rev. **130**, 1616 (1963).
[27] S. E. Rasmussen, K. S. Christensen, S. P. Pedersen, L. B. Kristensen, T. Bækkegaard, N. J. S. Loft, and N. T. Zinner, Superconducting circuit companion—an introduction with worked examples, PRX Quantum **2**, 040204 (2021).
[28] R. Kleiner, D. Koelle, F. Ludwig, and J. Clarke, Superconducting quantum interference devices: State of the art and applications, Proc. IEEE **92**, 1534 (2004).
[29] N. Frattini, U. Vool, S. Shankar, A. Narla, K. Sliwa, and M. Devoret, 3-wave mixing Josephson dipole element, Appl. Phys. Lett. **110**, 222603 (2017).
[30] W. Zhang, W. Huang, M. E. Gershenson, and M. T. Bell, Josephson metamaterial with a widely tunable positive or

negative Kerr constant, Phys. Rev. Appl. **8**, 051001(R) (2017).
[31] D. M. Basko, F. Pfeiffer, P. Adamus, M. Holzmann, and F. W. J. Hekking, Superconductor-insulator transition in Josephson junction chains by quantum monte carlo calculations, Phys. Rev. B **101**, 024518 (2020).
[32] See Supplemental Material at http://link.aps.org/supplemental/10.1103/g262-dlhf for the derivation of the action, a comment on the numerical methods, and results on other correlation functions not considered in the main text, which includes Refs. [33–35].
[33] G. Vidal, Classical simulation of infinite-size quantum lattice systems in one spatial dimension, Phys. Rev. Lett. **98**, 070201 (2007).
[34] R. Orús and G. Vidal, Infinite time-evolving block decimation algorithm beyond unitary evolution, Phys. Rev. B **78**, 155117 (2008).
[35] M. Fishman, S. R. White, and E. M. Stoudenmire, The ITensor software library for tensor network calculations, SciPost Phys. Codebases 4 (2022).
[36] The introduction of $\bar{v}_g$ is convenient for mapping length into time, though the physical results are independent of it.
[37] The dynamical variable ϕ_0 is the only independent degree of freedom as its conjugate momentum is proportional to ϕ_0^* [38]. Therefore, in Eq. (7) only derivatives of ϕ_0 appear.
[38] C. Cohen-Tannoudji, J. Dupont-Roc, and G. Grynberg, *Photons and Atoms: Introduction to Quantum Electrodynamics* (John Wiley & Sons, New York, 2024).
[39] Higher order corrections to the linear dispersion relation beyond the SVEA would give a momentum dependent mass.
[40] Note that the expansion of the action [Eq. (3)] to the lowest nonlinear order is enough to describe the strongly interacting gas, provided the field amplitude remains weak enough, i.e., $\phi/\Phi_0 \ll 1$. If needed, higher order terms would introduce multibody interaction terms in the Bose gas Hamiltonian.
[41] M. P. da Silva, D. Bozyigit, A. Wallraff, and A. Blais, Schemes for the observation of photon correlation functions in circuit QED with linear detectors, Phys. Rev. A **82**, 043804 (2010).
[42] C. Lang, D. Bozyigit, C. Eichler, L. Steffen, J. M. Fink, A. A. Abdumalikov, M. Baur, S. Filipp, M. P. da Silva, A. Blais, and A. Wallraff, Observation of resonant photon blockade at microwave frequencies using correlation function measurements, Phys. Rev. Lett. **106**, 243601 (2011).
[43] D. Bozyigit, C. Lang, L. Steffen, J. M. Fink, C. Eichler, M. Baur, R. Bianchetti, P. J. Leek, S. Filipp, M. P. da Silva, A. Blais, and A. Wallraff, Antibunching of microwave-frequency photons observed in correlation measurements using linear detectors, Nat. Phys. **7**, 154 (2011).
[44] C. Cohen-Tannoudji, J. Dupont-Roc, and G. Grynberg, *Atom-Photon Interactions: Basic Processes and Applications* (John Wiley & Sons, New York, 2024).
[45] A. Polkovnikov and V. Gritsev, Breakdown of the adiabatic limit in low-dimensional gapless systems, Nat. Phys. **4**, 477 (2008).
[46] A. Ergül, T. Weißl, J. Johansson, J. Lidmar, and D. B. Haviland, Spatial and temporal distribution of phase slips in Josephson junction chains, Sci. Rep. **7**, 11447 (2017).
[47] R. Behr, O. Kieler, J. Kohlmann, F. Müller, and L. Palafox, Development and metrological applications of Josephson arrays at ptb, Meas. Sci. Technol. **23**, 124002 (2012).
[48] T. Langen, R. Geiger, M. Kuhnert, B. Rauer, and J. Schmiedmayer, Local emergence of thermal correlations in an isolated quantum many-body system, Nat. Phys. **9**, 640 (2013).
[49] P. Calabrese and J. Cardy, Time dependence of correlation functions following a quantum quench, Phys. Rev. Lett. **96**, 136801 (2006).
[50] S. Frasca, C. Roy, G. Beaulieu, and P. Scarlino, Three-wave-mixing quantum-limited kinetic inductance parametric amplifier operating at 6 T near 1 K, Phys. Rev. Appl. **21**, 024011 (2024).
[51] P. M. Walker, L. Tinkler, M. Durska, D. M. Whittaker, I. J. Luxmoore, B. Royall, D. N. Krizhanovskii, M. S. Skolnick, I. Farrer, and D. A. Ritchie, Exciton polaritons in semiconductor waveguides, Appl. Phys. Lett. **102**, 012109 (2013).
[52] D. G. Suárez-Forero, F. Riminucci, V. Ardizzone, N. Karpowicz, E. Maggiolini, G. Macorini, G. Lerario, F. Todisco, M. De Giorgi, L. Dominici, D. Ballarini, G. Gigli, A. S. Lanotte, K. West, K. Baldwin, L. Pfeiffer, and D. Sanvitto, Enhancement of parametric effects in polariton waveguides induced by dipolar interactions, Phys. Rev. Lett. **126**, 137401 (2021).
[53] I. Rosenberg, D. Liran, Y. Mazuz-Harpaz, K. West, L. Pfeiffer, and R. Rapaport, Strongly interacting dipolar-polaritons, Sci. Adv. **4**, eaat8880 (2018).
[54] M. Horvath, A. Bastianello, S. Dhar, R. Koch, Y. Guo, J.-S. Caux, M. Landini, and H.-C. Nägerl, Observing Bethe strings in an attractive Bose gas far from equilibrium, arXiv:2505.10550.
[55] C. Oliver, S. Mukherjee, M. C. Rechstman, I. Carusotto, and H. M. Price, Artificial gauge fields in the t-z mapping for optical pulses: Spatiotemporal wave packet control and quantum Hall physics, Sci. Adv. **9**, eadj0360 (2023).
[56] J. Monroe, D. Kowsari, K. Zheng, C. Gaikwad, J. Brewster, D. Wisbey, and K. Murch, Optical direct write of Dolan–Niemeyer-bridge junctions for transmon qubits, Appl. Phys. Lett. **119**, 062601 (2021).
[57] R. Zhao, S. Park, T. Zhao, M. Bal, C. R. J. McRae, J. Long, and D. P. Pappas, Merged-element transmon, Phys. Rev. Appl. **14**, 064006 (2020).
[58] P. Manset, J. Palomo, A. Schmitt, K. Gerashchenko, R. Rousseau, H. Patange, P. Abgrall, E. Flurin, S. Deléglise, T. Jacqmin, and L. Balembois, Hyperinductance based on stacked Josephson junctions, arXiv:2505.02764.
[59] L. Planat, A. Ranadive, R. Dassonneville, J. Puertas Martínez, S. Léger, C. Naud, O. Buisson, W. Hasch-Guichard, D. M. Basko, and N. Roch, Photonic-crystal Josephson traveling-wave parametric amplifier, Phys. Rev. X **10**, 021021 (2020).

End Matter

Dependence of Bose gas properties on circuit parameters—The explicit forms of the physical quantities in Eqs. (7) and (10) are as follows. The overall normalization of the action is

$$\mathcal{C} = \frac{r\sqrt{-(1+4c)r^2+4c}}{\hbar c L_J \bar{v}_g}. \tag{A1}$$

The group velocity is

$$v_g = \frac{\omega_P}{2} a\sqrt{-(1+4c)r^2+4c}(1-r^2). \tag{A2}$$

The mass and interaction constant of the one-dimensional Bose gas are

$$m = -\frac{\omega_P^2}{2}\frac{a\hbar}{\bar{v}_g^3 r}\frac{[-(1+4c)r^2+4c]^{3/2}(1-r^2)}{1+12c-\frac{2r^2}{1-r^2}} \quad \text{and}$$
$$g = -\left(\frac{2\pi}{\Phi_0}\right)^2 \frac{\hbar^2 \bar{v}_g^2 L_J}{2a}\frac{r^2}{[-(1+4c)r^2+4c](1-r^2)^2}. \tag{A3}$$

Here, we used the shorthand $r = \omega_0/\omega_P$, $\omega_P = 1/\sqrt{L_J C_J}$, and $c = C_J/C_0$.

The density of the Bose gas can be derived from the incoming photon flux $\Phi_{\rm ph}$ by noting that the energy per unit length transported by incoming photons traveling at v_g is $\mathcal{E}_1 = \hbar\omega_0\Phi_{\rm ph}/v_g$. This must equal the energy density computed from Eq. (1) for a plane wave in the linear regime. Imposing a plane-wave form of ϕ_n, inserting it into the Hamiltonian corresponding to the Lagrangian of Eq. (1), and expressing the resulting energy in terms of the expectation value of the Bose field $\hat{\Psi}$ of Eq. (9), we get $\mathcal{E}_2 = \hbar\omega_0\bar{v}_g|\Psi|^2/v_g$, which immediately implies that $\rho = |\Psi|^2 = \Phi_{\rm ph}/\bar{v}_g$.

Validity of approximations—As explained above, our approach is based on expanding the linear dispersion relation up to second order around the carrier at (k_0, ω_0). This SVEA approximation must hold throughout the full propagation and in particular in the TG regime. As the spread in frequency of the TG ground state is given by $\Delta\omega = \pi\Phi_{\rm ph}$, the condition for the third order dispersion term to be negligible reads as

$$\frac{1}{2}\left|\frac{\partial^2 k}{\partial\omega^2}\right|_{k_0} \gg \frac{\pi}{6}\left|\frac{\partial^3 k}{\partial\omega^3}\right|_{k_0}\Phi_{\rm ph}. \tag{B1}$$

The ratio of these two quantities is plotted in Fig. 4(a): the fact that it is indeed much smaller than one for the chosen parameters validates our approximation.

In Fig. 4(b) we plot the maximum relative variation of the interaction constant g in the spectral region $\Delta\omega$ of interest: while the variation is moderate but significant, it is not expected to impact the validity of our findings since a slight variation of the interaction strength does not affect the overall many-body properties of the TG gas.

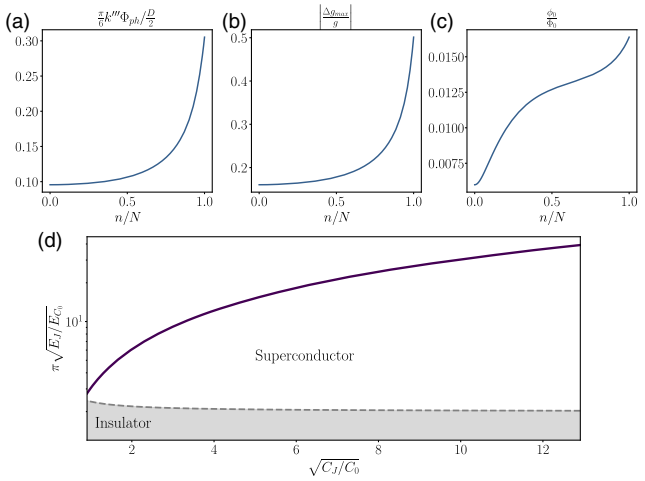


FIG. 4. Validity of the approximations. First correction to parabolic dispersion (a), variation of the contact interaction parameter (b), and field amplitude (c). (d) Phase diagram of the transmission line as in Ref. [31]. The solid line represents the chosen parameters for the tapered transmission line. Parameters are as in Figs. 2(a) and 2(b) in the main text.

Moreover, in Fig. 4(c) we show the field amplitude ϕ_0/Φ_0: its small value supports our expansion of the cosine in Eq. (1) up to the quartic term only.

Finally, in Fig. 4(d) we show the phase diagram of the transmission line as a function of the ratio of the two capacitances and of the Josephson $E_J = \Phi_0^2/(4\pi^2 L_J)$ and charging $E_{C_0} = (2e)^2/C_0$ energies, as computed in Ref. [31], and we show that we always lie on the superconducting side along the whole transmission line.

Effect of a finite interaction constant γ—In Fig. 2 of the main text, we showed the numerically calculated correlation functions of the field after the ramp. The ground state correlation function at finite γ was computed by means of an imaginary time evolution on the infinite-MPS ansatz [34]. In Fig. 5, the result for a

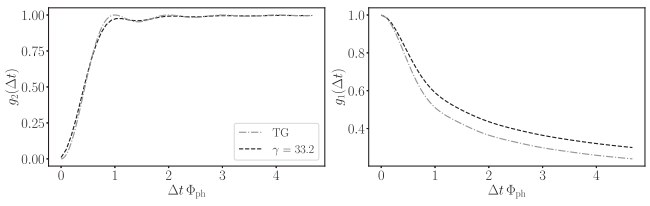


FIG. 5. First (left) and second (right) order correlation functions in the TG limit (gray dashed-dotted line) and for the finite $\gamma \approx 33.2$ (black dashed line) used in the text.

value $\gamma \approx 33.2$ corresponding to the end of the ramp is compared to the predictions for the TG gas at $\gamma \to \infty$. The good agreement of the curves show that for this value of γ we are already well into the TG regime. The only qualitative effect of the finite γ is a slight reduction of the amplitude of the Friedel oscillations.

Comment on experimental feasibility—In this section, we comment on the experimental feasibility of the proposed experiment.

Sampling rate for $g_{1,2}(\Delta t)$:First, fast resolution around 2–3 ns is required to resolve features in the pair correlation functions shown in the main text. While experimental observations so far [41,42] report a resolution of around 10 ns, the slight increase of the sampling rate that is needed to resolve these features is well within the possibility of state-of-the-art electronics. This comes at the price of increasing the noise bandwidth. The ensuing reduction of the signal to noise ratio can be compensated with a longer sampling time, allowing for detecting small features like the Friedel oscillations. Alternatively, one may also consider increasing the characteristic timescale of the correlation features, which is inversely proportional to the incident photon flux. As this comes with the price of a smaller characteristic energy, a compromise would need to be taken with the device length to preserve adiabaticity.

Range for the plasma frequency: While the proposed value of 5 GHz for the plasma frequency is lower than the typical parameters for Josephson junctions (JJs), high-L_J junctions with low plasma frequencies in this range have been fabricated in state-of-the-art devices [56–58]. Moreover, replacing simple JJs with more sophisticated geometries such as SQUIDs or SNAILs [28,29] enables a further reduction of the effective plasma frequency by exploiting their flux tunability.

Number of cells: We note that, for the specific ramp that we considered, a transmission line with a number $N \approx 8.8 \times 10^4$ of cells is largely sufficient to adiabatically generate a Tonks-Girardeau gas close to its ground state. While this value is around an order of magnitude larger than the currently existing waveguide devices [46], it is well comparable to the one of Josephson arrays for metrological applications [47]. Furthermore, the constraint on the device length can be loosened by further reducing the effective plasma frequency, as explained in the main text, or by engineering the linear dispersion relation in order to reduce the effective mass m of the Bose gas. This can be done, for example, by considering a two-site unit cell and periodically modulating the junction parameters [59].

Effect of the photon losses and disorder: In an actual experimental setup, losses, though small, are generally unavoidable. Their main effect in our fermionized system is to heat up the gas, due to the fact that losing a fermion creates a hole excitation in the Fermi sphere. An upper bound on the excitation energy resulting from a fractional intensity drop of $\beta = 1 - I_f/I_i$, can be estimated assuming that all particles are lost at the center of the Fermi sphere. This gives $\Delta E/E_0 = 3\beta/(1-\beta)^2$. From this we expect that a typical temperature of $T \sim 0.2T_F$, for which Friedel oscillations are damped by a factor of 2, results from a loss of $\beta \approx 6\%$. We note that this is a worst-case estimate, as losses occurring during the initial part of the propagation do not actually result in gas heating due to the coherent nature of the photon gas in the early stages of propagation. Finally, we expect that a small disorder along the transmission line does not result in a sizeable heating of the gas as disorder corresponds to a small shaking of the gas parameters on extremely fast timescales, which is therefore averaged out.